

The Distribution of Dark Matter in Galaxies: Constant–Density Dark Halos Envelop the Stellar Disks

Paolo Salucci¹ and Annamaria Borriello¹

(1) International School for Advanced Studies SISSA-ISAS – Trieste, I

Abstract. In this paper we review the main and the most recent evidence for the presence of a core radius in the distribution of the dark matter around spiral galaxies. Their rotation curves, coadded according to the galaxy luminosity, conform to an Universal profile which can be represented as the sum of an exponential thin disk term plus a spherical halo term with a flat density core. From dwarfs to giants, these halos feature a constant density region of size r_0 and core density ρ_0 related by $\rho_0 = 4.5 \times 10^{-2} (r_0/\text{kpc})^{-2/3} M_\odot \text{pc}^{-3}$. At the highest masses ρ_0 decreases exponentially, with r_0 revealing a lack of objects with disk masses $> 10^{11} M_\odot$ and central densities $> 1.5 \times 10^{-2} (r_0/\text{kpc})^{-3} M_\odot \text{pc}^{-3}$, which implies a *maximum* mass of $\approx 2 \times 10^{12} M_\odot$ for halos hosting spirals. The fine structure of dark matter halos is obtained from the kinematics of a number of suitable low-luminosity disk galaxies. The inferred halo circular velocity increases linearly with radius out to the edge of the stellar disk, implying a constant dark halo density over the entire disk region. The structural properties of halos around normal spirals are similar to those around dwarf and low surface brightness galaxies; nevertheless they provide far more substantial evidence of the discrepancy between the mass distributions predicted in the Cold Dark Matter scenario and those actually detected around galaxies.

1 Introduction

Rotation curves (RC's) of disk galaxies are the best probe for dark matter (DM) on galactic scale. Notwithstanding the impressive amount of knowledge gathered in the past 20 years, only very recently we start to shed light to crucial aspects of the mass *distribution* including the actual density profile of dark halos and its claimed universality.

On the cosmological side, high-resolution cosmological N-body simulations have shown that cold dark matter (CDM) halos achieve a specific equilibrium density profile [16 hereafter NFW, 6, 10, 14, 11]. This can be characterized by one free parameter, e.g. M_{200} , the halo mass contained within the radius inside which the average over-density is 200 times the critical density of the Universe at the formation epoch. In their innermost region the dark matter profiles show some scatter around an average profile which is characterized by a power-law cusp $\rho \sim r^{-\gamma}$, with $\gamma = 1 - 1.5$ [16, 14, 2]. In detail, the DM density profile is:

$$\rho_{\text{NFW}}(r) = \frac{\rho_s}{(r/r_s)(1+r/r_s)^2} \quad (1)$$

where r_s is a characteristic inner radius and ρ_s the corresponding density. Let us define the halo virial radius R_{vir} as the radius within which the mean density is Δ_{vir} times the mean universal density ρ_m at that redshift, and the associated virial mass M_{vir} and velocity $V_{\text{vir}} \equiv GM_{\text{vir}}/R_{\text{vir}}$. By defining the concentration parameter as $c_{\text{vir}} \equiv R_{\text{vir}}/r_s$ the halo circular velocity $V_{\text{CDM}}(r)$ takes the form [2]:

$$V_{\text{CDM}}^2(r) = V_{\text{vir}}^2 \frac{c_{\text{vir}}}{A(c_{\text{vir}})} \frac{A(x)}{x} \quad (2)$$

where $x \equiv r/r_s$ and $A(x) \equiv \ln(1+x) - x/(1+x)$. As the relation between V_{vir} and R_{vir} is fully specified by the background cosmology, we assume the currently popular Λ CDM cosmological model, with $\Omega_m = 0.3$, $\Omega_\Lambda = 0.7$ and $h = 0.75$, in order to reduce from three to two (c_{vir} and r_s) the independent parameters characterizing the model. According to this model, $\Delta_{\text{vir}} \simeq 340$ at $z \simeq 0$. Let us stress that a high density $\Omega_m = 1$ model, with a concentration parameter $c_{\text{vir}} > 12$, is definitely unable to account for the observed galaxy kinematics [13]. Until recently, due to both the limited number of suitable RC's and to uncertainties on the exact amount of luminous matter in the innermost regions of spirals, it has been difficult to investigate the internal structure of their dark halos. However, as a result of substantial observational and theoretical progresses, we have recently derived the main features of their mass distribution for *a*) the Universal Rotation Curve [20] built by coadding 1000 RC's and *b*) a number of suitably selected RC's [1].

2 The URC and CDM Halos

The assumed (and well supported) framework is: *a*) the mass in spirals is distributed according to the Inner Baryon Dominance (IBD) regime: there is a characteristic transition radius $R_{IBD} \simeq 2R_d(V_{opt}/220 \text{ km/s})^{1.2}$ (R_d is the disk scale-length and $V_{opt} \equiv V(R_{opt})$) according which, for $r \leq R_{IBD}$, the luminous matter totally accounts for the mass distribution, whereas, for $r > R_{IBD}$, DM *rapidly* becomes the dominant dynamical component [26, 24, 1]. Then, although the dark halo might extend down to the galaxy center, it is only for $r > R_{IBD}$ that it gives a non-negligible contribution to the circular velocity. *b*) DM is distributed in a different way with respect to any of the various baryonic components [20, 7], and *c*) HI contribution to the circular velocity at $r < R_{opt}$, is negligible [e.g. 21].

2.1 Halo Density Profiles

Reference [20] have derived from 15000 velocity measurements of 1000 RC's, the synthetic rotation velocities of spirals $V_{syn}(\frac{r}{R_{opt}}, \frac{L_I}{L_*})$, sorted by luminosity (Fig. 1, with L_I the I -band luminosity and $L_I/L_* = 10^{-(M_I+21.9)/5}$). Remarkably, *individual* RC's have a very small variance with respect to the corresponding synthetic curves [20, 21, 22]: spirals sweep a very narrow locus in the

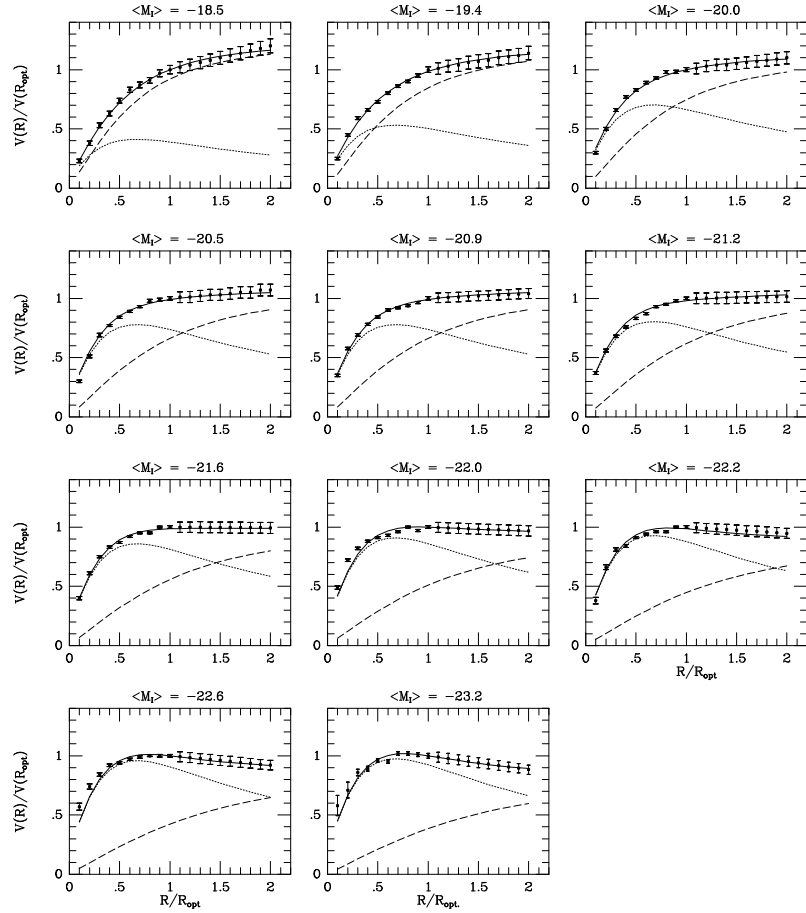


Fig. 1. Synthetic rotation curves (filled circles with error bars) and URC (solid line) with its separate dark/luminous contributions (dotted line: disk; dashed line: halo). See [20] for details

RC-profile/amplitude/luminosity space. On the other hand, the galaxy kinematical properties significantly change with luminosity [e.g. 20], so it is natural to relate the mass distribution with this quantity. The whole set of synthetic RC's has been reproduced by means of the Universal Rotation Curve (URC) $V_{URC}(r/R_{opt}, L_I/L_*)$ which includes: a) an exponential thin disk term [9]:

$$V_{d,URC}^2(x) = 1.28 \beta V_{opt}^2 x^2 (I_0 K_0 - I_1 K_1)|_{1.6x} \quad (3)$$

and b) a spherical halo term:

$$V_{h,URC}^2(x) = V_{opt}^2 (1 - \beta) (1 + a^2) \frac{x^2}{(x^2 + a^2)}, \quad (4)$$

with $x \equiv r/R_{opt}$, $\beta \equiv (V_{d,URC}(R_{opt})/V_{opt})^2$, $V_{opt} \equiv V(R_{opt})$ and a the halo core radius in units of R_{opt} . At high luminosities, the contribution from a bulge component has also been considered.

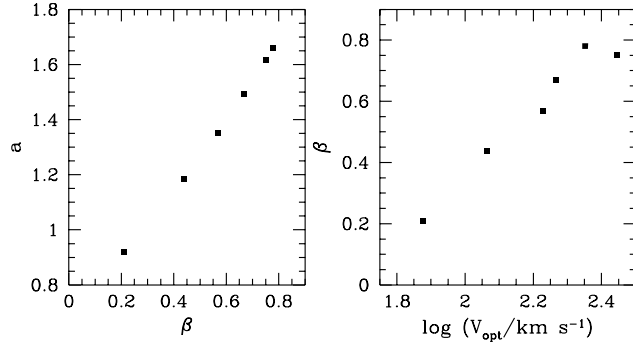


Fig. 2. a vs β and β vs V_{opt}

Let us stress that the halo velocity functional form (4) does not bias the mass model: it can equally account for maximum-disk, solid-body, no-halo, all-halo, CDM and core-less halo mass models. In practice, the synthetic curves V_{syn} select the actual model out of the family of models $V_{URC}^2(x) = V_{h,URC}^2(x, \beta, a) + V_{d,URC}^2(x, \beta)$, where a and β are free parameters. Adopting $a \simeq 1.5(L_I/L_*)^{1/5}$ and $\beta \simeq 0.72 + 0.44 \log(L_I/L_*)$ [20] or, equivalently, the corresponding $a = a(\beta)$ and $\beta = \beta(\log V_{opt})$ plotted in Fig. 2, the URC reproduces the synthetic curves $V_{syn}(r)$ within their r.m.s. (see Fig. 1). More in detail, at any luminosity and radius, $|V_{URC} - V_{syn}| < 2\%$ and the 1σ fitting uncertainties on a and β are about 20% [20].

To cope with this observational evidence and conveniently frame the halo density properties, we adopted the empirical profile proposed by Burkert [3]:

$$\rho_b(r) = \frac{\rho_0 r_0^3}{(r + r_0)(r^2 + r_0^2)} \quad (5)$$

where ρ_0 and r_0 are free parameters which represent the central DM density and the scale radius. Within spherical symmetry, the mass distribution is given by:

$$M_b(r) = 4M_0 \{ \ln(1 + r/r_0) - \arctan(r/r_0) + 0.5 \ln[1 + (r/r_0)^2] \} \quad (6)$$

with M_0 , the dark mass within the core, given by $M_0 = 1.6\rho_0 r_0^3$. The halo contribution to the circular velocity is then:

$$V_b^2(r) = GM_b(r)r \quad (7)$$

Although the dark matter core parameters r_0 , ρ_0 and M_0 are in principle independent, the observations reveal a clear correlation [3]:

$$M_0 = 4.3 \times 10^7 \left(\frac{r_0}{kpc} \right)^{7/3} M_\odot \quad (8)$$

which, together with the above relationship, indicates that dark halos represent a 1-parameter family which is completely specified, e.g. by the core mass.

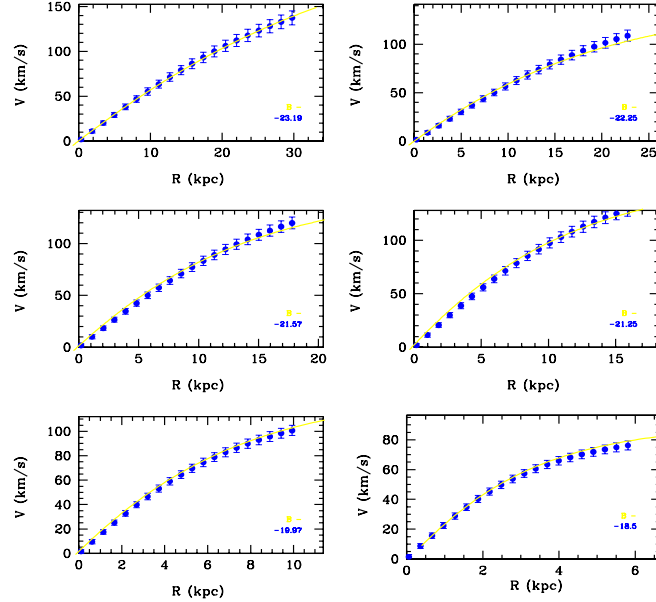


Fig. 3. URC-halo rotation curves (*filled circles* with error bars) and the Burkert model (*solid line*). The bin magnitudes are also indicated

We then compare the dark halo velocities obtained with (3) and (4), with the Burkert velocities $V_b(r)$ of (5)-(7), leaving ρ_0 and r_0 as free parameters, i.e. we do not impose the relationship (8). The results are shown in Fig. 3: at any luminosity, out to the outermost radii ($\sim 6R_d$), $V_b(r)$ is indistinguishable from $V_{h,URC}(r)$. More specifically, by setting $V_{h,URC}(r) \equiv V_b(r)$, we are able to reproduce the synthetic rotation curves $V_{syn}(r)$ at the level of their r.m.s. For $r \gg 6R_d$, i.e. beyond the region described by the URC, the two velocity profiles progressively differ.

The values of r_0 and ρ_0 from the URC agree with the extrapolation at high masses of the scaling law $\rho \propto r_0^{-2/3}$ [3] established for objects with core radii r_0 ten times smaller (see Fig. 4). Let us notice that the core radii are very large: $r_0 \gg R_d$ so that an ever-rising halo RC cannot be excluded by the data. Moreover, the disk-mass vs. central halo density relationship $\rho_0 \propto M_d^{-1/3}$, found

for dwarf galaxies [3], according to which the densest halos harbor the least massive disks, holds also for disk systems of stellar mass up to $10^{11}M_{\odot}$ (see Fig. 4).

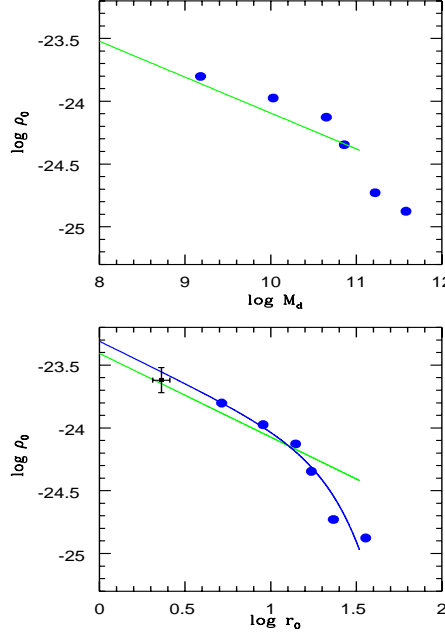


Fig. 4. (up) Disk mass (in solar units) *vs* central halo density ρ_0 (in g/cm^3) for normal spirals (*filled circles*). The straight line is from [3]. (bottom) central density *vs* core radii (in kpc) for normal spirals (*filled circles*). The straight line and the point are from the dwarfs sample of [3]. The curved line is: $\rho_0 = 5 \times 10^{-24} r_0^{-2/3} \exp(-(r_0/27)^2 g/cm^3$.

The above relationship shows a curvature at the highest masses/lowest densities that can be related to the existence of an upper limit in the dark halo mass M_{200} ¹ which is evident by the sudden decline of the baryonic *mass* function of disk galaxies at $M_d^{max} = 2 \times 10^{11} M_{\odot}$ [26], that implies a maximum halo mass of $M_{200}^{max} \sim \Omega_0/\Omega_b M_d^{max}$, where Ω_0 and $\Omega_b \simeq 0.03$ [e.g. 5] are the matter and baryonic densities of the Universe in units of critical density. From the definition of M_{200} , by means of eq. (6) and (8), we can write M_{200} in terms of the “observable” quantity M_0 : $M_{200} = \eta M_0$. For $(\Omega_0, z) = (0.3, 3)$, $\eta \simeq 12$; notice that there is a mild dependence of η on z and Ω_0 which is irrelevant for the present study. From simple manipulation of previous equation- we obtain an upper limit for the central density, $\rho_0 < 1 \times 10^{-20} (r_0/\text{kpc})^{-3} g/cm^3$, which implies a lack

¹ The virial halo mass is given by $M_{200} \equiv 200 \times 4\pi/3 \rho_c R_{200}^3 \Omega_0 (1+z^3) g(z)$ with z the formation redshift, R_{200} the virial radius, for $g(z)$ see e.g. [2]; the critical density is defined as: $\rho_c \equiv 3/(8\pi) G^{-1} H_0^2$.

of objects with $\rho_0 > 4 \times 10^{-25} \text{ g/cm}^3$ and $r_0 > 30 \text{ kpc}$, as is evident in Fig. 4. Turning the argument around, the deficit of objects with $M_d \sim M_d^{max}$ and $\rho_0 > 4 \times 10^{-25} \text{ g/cm}^3$, suggests that, at this mass scale, the total-to-baryonic density ratio nears the cosmological value $\Omega/\Omega_b \simeq 10$.

2.2 Testing CDM

Out to two optical radii, the Burkert density profile reproduces, for the whole spiral luminosity sequence, the DM halos mass distribution. This density profile, though at very large radii coincides with the NFW profile, approaches a constant, finite density value at the center, in a way consistent with an isothermal distribution. This is in contradiction to CDM halo properties which predict [e.g. 10] that the velocity dispersion σ of the dark matter particles decreases towards the center to reach $\sigma \rightarrow 0$ for $r \rightarrow 0$. The dark halo inner regions, therefore, cannot be considered as kinematically cold structures but rather as “warm” regions with size $r_0 \propto \rho_0^{-1.5}$. The halo core sizes are very large: $r_0 \sim 4 - 7R_d$. Then, the boundary of the core region is well beyond the region where the stars are located and, as in [7], even at the outermost observed radius there is not the slightest evidence that dark halos converge to a $\rho \sim r^{-2}$ (or a steeper) regime.

3 Individual RC’s and CDM

To derive the halo density from an individual rotation curve is certainly complicated, however, the belief according to which RC’s lead to ambiguous halo mass modeling [e.g. 28] is incorrect. In fact this is true only for rotation curves of low spatial resolution, i.e. with < 3 measures per exponential disk length-scale R_d , as for most of HI RCs. Since the parameters of the galaxy structure are very sensitive to the *shape* of the rotation curve in the region $0 < r < R_d$, that corresponds to the region of the RC steepest rise, then the mass model cannot be inferred if such a region is poorly sampled and/or radio beam-biased. Instead, high-quality *optical* RCs with tens of independent measurements in the critical region probe the halo mass distribution and resolve their structure. Since the dark component can be better traced when the disk contributes to the dynamics in a modest way, it is convenient to investigate DM-dominated objects, like dwarf and low surface brightness (LSB) galaxies. It is well known that for the latter there are claims of dark matter distributions with regions of constant density well different from the cusped density distributions of the Cold Dark Matter scenario [e.g. 8, 13, 3, 4, 11, 12, 27]. However, these results are far from certain being 1) under the (unlikely) *caveat* that the low spatial resolution of the RCs does not bias the derived mass model and 2) uncertain, due to the limited amount of available kinematical data [see 29]. Since most of the properties of cosmological halos are claimed universal, we concentrate on a small and particular sample of RCs, that, nevertheless, reveal the properties of the DM halos around spirals. A more useful strategy has been to investigate a number of high-quality *optical* rotation curves of *low luminosity* late-type spirals, with

I -band absolute magnitudes $-21.4 < M_I < -20.0$ and that $100 < V_{opt} < 170$ km s $^{-1}$. Objects in this luminosity/velocity range are DM dominated [e.g. 20] but their RC's, measured at an angular resolution of 2'', have a spatial resolution of $w \sim 100(D/10$ Mpc) pc and $n_{data} \sim R_{opt}/w$ independent measurements. For nearby galaxies: $w \ll R_d$ and $n_{data} > 25$. Moreover, we select RC's of bulge-less systems, so that the stellar disk is the only baryonic component for $r \lesssim R_d$.

In detail, we take from [19] the rotation curves of the ‘excellent’ subsample of 80 galaxies, which are suitable for an accurate mass modeling. In fact, these RC's properly trace the gravitational potential in that: 1) data extend at least to the optical radius, 2) they are smooth and symmetric, 3) they have small r_{rms} , 4) they have high spatial resolution and a homogeneous radial data coverage, i.e. about 30 – 100 data points homogeneously distributed with radius and between the two arms. From this subsample we extract 9 rotation curves of low luminosity galaxies ($5 \times 10^9 L_\odot < L_I < 2 \times 10^{10} L_\odot$; $100 < V_{opt} < 170$ km s $^{-1}$), with their I -band surface luminosity being an (almost) perfect radial exponential. These two last criteria, not indispensable to perform the *mass* decomposition, are however required to infer the dark halo *density* distribution. Each RC has 7 – 15 velocity points inside R_{opt} , each one being the average of 2 – 6 independent data. The RC spatial resolution is better than $1/20 R_{opt}$, the velocity r.m.s. is about 3% and the RC's logarithmic derivative is generally known within about 0.05.

3.1 Halo Density Profiles

We model the mass distribution as the sum of two components: a stellar disk and a spherical dark halo. By assuming centrifugal equilibrium under the action of the gravitational potential, the observed circular velocity can be split into these two components:

$$V^2(r) = V_D^2(r) + V_H^2(r) \quad (9)$$

By selection, the objects are bulge-less and the stellar component is distributed like an exponential thin disk. Light traces the mass via an assumed radially constant mass-to-light ratio. In the r.h.s of (9) we neglect the gas contribution $V_{gas}(r)$ since in normal spirals it is usually modest within the optical region [21, Fig. 4.13]: $\beta_{gas} \equiv (V_{gas}^2/V^2)_{R_{opt}} \sim 0.1$. Furthermore, high resolution HI observations show that in low luminosity spirals: $V_{gas}(r) \simeq 0$ for $r < R_d$ and $V_{gas}(r) \simeq (20 \pm 5)(r - R_d)/2R_d$ for $R_d \leq r \leq 3R_d$. Thus, in the optical region: *i*) $V_{gas}^2(r) \ll V^2(r)$ and *ii*) $d[V^2(r) - V_{gas}^2(r)]/dr \gtrsim 0$. This last condition implies that by including V_{gas} in the r.h.s. of (9) the halo velocity profiles would result *steeper* and then the core radius in the halo density *larger*. Incidentally, this is not the case for dwarfs and LSBs: most of their kinematics is affected by the HI disk gravitational pull in such a way that neglecting it could bias the determination of the DM density. The circular velocity profile of the disk is given by (3) and the DM halo will have the form given by (4). Since we normalize (at R_{opt}) the velocity model $(V_h^2 + V_d^2)^{1/2}$ to the observed rotation speed V_{opt} , β enters

explicitly in the halo velocity model and this reduces the free parameters of the mass model to two.

It is important to remark that, out to R_{opt} , the proposed Constant Density Region (CDR) mass model of (4) is instead *neutral* with respect to all the proposed models. Indeed, by varying β and a , we can efficiently reproduce the maximum-disk, the solid-body, the no-halo, the all-halo, the CDM and the core-less-halo models. For instance, CDM halos with concentration parameter $c = 5$ and $r_s = R_{opt}$ are well fit by (4) with $a \simeq 0.33$.

For each galaxy, we determine the values of the parameters β and a by means of a χ^2 -minimization fit to the observed rotation curves:

$$V_{model}^2(r; \beta, a) = V_d^2(r; \beta) + V_d^2(r; \beta, a) \quad (10)$$

A central role in discriminating among the different mass decompositions is played by the derivative of the velocity field dV/dr . It has been shown [e.g. 18] that by taking into account the logarithmic gradient of the circular velocity field defined as: $\nabla(r) \equiv \frac{d \log V(r)}{d \log r}$ one can retrieve the crucial information stored in the shape of the rotation curve. Then, we set the χ^2 -s as the sum of those evaluated on velocities and on logarithmic gradients: $\chi_V^2 = \sum_{i=1}^{n_V} \frac{V_i - V_{model}(r_i; \beta, a)}{\delta V_i}$ and $\chi_{\nabla}^2 = \sum_{i=1}^{n_{\nabla}} \frac{\nabla(r_i) - \nabla_{model}(r_i; \beta, a)}{\delta \nabla_i}$, with $\nabla_{model}(r_i, \beta, a)$ given from the above equations. The parameters of the mass models are finally obtained by minimizing the quantity $\chi_{tot}^2 \equiv \chi_V^2 + \chi_{\nabla}^2$.

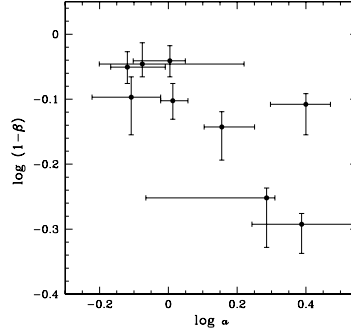


Fig. 5. Halo parameters (a is in units of R_{opt}) with their uncertainties

The parameters of the best-fit models are shown in Fig. 5. They are very well specified: the allowed values span a small and continuous region of the (a, β) space. We get a “lowest” and a “highest” halo velocity curve by subtracting from $V(r)$ the maximum and the minimum disk contributions $V_d(r)$ obtained by substituting in (3) the parameter β with $\beta_{best} + \delta\beta$ and $\beta_{best} - \delta\beta$, respectively. The derived mass models are shown in Fig. 6, alongside with the separate disk and halo contributions. It is then obvious that the halo curve is steadily increasing, almost linearly, out to the last data point. The disk-contribution β and the

halo core radius a span a range from 0.1 to 0.5 and from 0.8 to 2.5, respectively. In each object the uniqueness of the resulting halo velocity model can be realized by the fact that the maximum-disk and minimum-disk models almost coincide. Remarkably, we find that the size of the halo density core is always greater than the disk characteristic scale-length R_d and it can extend beyond the disk edge (and the region investigated).

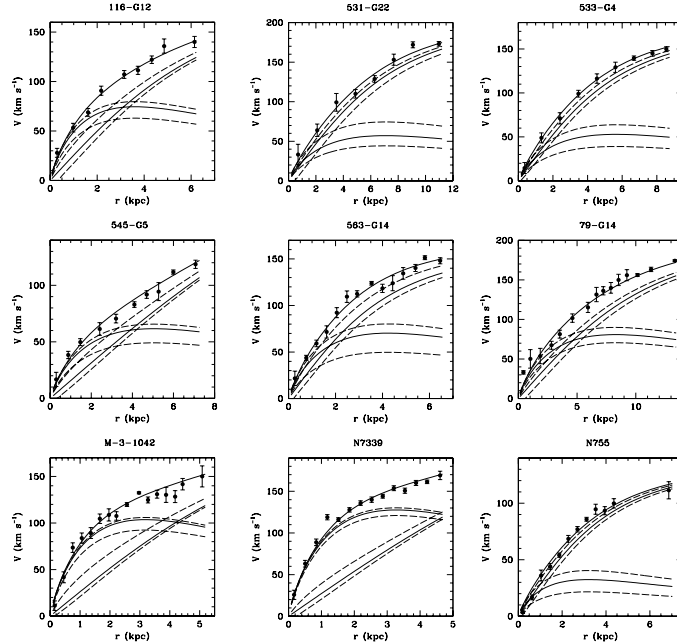


Fig. 6. CDR model fits (thick solid line) to the RCs (points with errorbars). Thin solid lines represent the disk and halo contributions. The maximum disk and the minimum disk solutions are also plotted (dashed lines)

3.2 Testing CDM

In Fig. 7 we show the halo velocity profiles for the nine galaxies. The halo circular velocities are normalized to their values at R_{opt} and expressed as a function of the normalized radius r/R_{opt} . These normalizations allow a meaningful comparison between halos of different masses. It is then evident that the halo circular velocity, in every galaxy, rises almost linearly with radius, at least out to the disk edge: $V_h(r) \propto r$ for $0.05R_{opt} \lesssim r \lesssim R_{opt}$.

The halo density profile has a well defined (core) radius within which the density is approximately constant. This is inconsistent with the singular halo

density distribution emerging in the Cold Dark Matter (CDM) halo formation scenario. More precisely, since the CDM halos are, at small radii, likely more cuspy than the NFW profile: $\rho_{CDM} \propto r^{-1.5}$ [e.g. 14], the steepest CDM halo velocity profile $V_h(r) \propto r^{1/4}$ results too shallow with respect to observations. Although the mass models of (4) converge to a distribution with an inner core rather than with a central spike, it is worth, given the importance of such result, also checking in a direct way the (in)compatibility of the CDM models with galaxy kinematics. We assume the NFW two-parameters functional form for the halo density [15, 16, 17], given by (1). Though N-body simulations and semi-analytic investigations indicate that the two parameters c_{vir} and r_s correlate, they are left independent to increase the chance of a good fit. For the object under study a generous halo mass M_{vir} upper limit is $M_{up} = 2 \times 10^{12} M_\odot$.

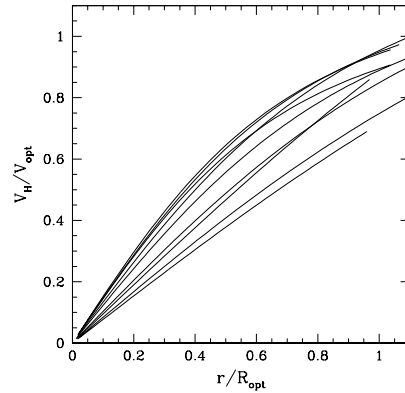


Fig. 7. The halo velocity profiles of the sample spirals. $V_h(r)$ rises almost linearly with radius: the DM halo density remains approximately constant

The fits to the data are shown in Fig. 8 and compared with the NFW models: for seven out of nine objects the latter are unacceptably worse than the CDR solutions, moreover in all objects, the CDM virial mass is too high: $M_{vir} \sim 2 \times 10^{12} M_\odot$ and the resulting disk mass-to-light ratio too low. The inadequacy of the CDM model for our sample galaxies is even more evident if one performs the fit after removing the constraint on virial mass. In fact, good fits are obtained only for very low values of the concentration parameter ($c_{vir} \simeq 2$) and for ridiculously large virial velocities and masses ($V_{vir} \simeq 600-800 \text{ km s}^{-1}$; $M_{vir} \simeq 10^{13} - 10^{14} M_\odot$). These results can be explained as effect of the attempt, by the minimization routine, to fit the NFW velocity profile ($V(r) \propto r^{0.5}$) to data intrinsically linear in r .

4 Conclusions: an Intriguing Evidence

The dark halos around spirals emerge as an one-parameter family; it is relevant that the order parameter (either the central density or the core radius) corre-

lates with the luminous mass. However, we do not know how it is related to the global structural properties of the dark halo, like the virial radius or the virial mass. The halo RC, out to $6R_d$, is completely determined by parameters, i.e. the central core density and the core radius, which are not defined in present gravitational instability/ hierarchical clustering scenario. In fact the location of spiral galaxies in the parameter space of virial mass, halo central density and baryonic mass, determined by different processes on different scales, degenerates with no doubt into a single curve (see Fig. 4), we recall that: $\rho_0 = \frac{\pi}{24} M_{200}/r_0^3$ and $M_d = G^{-1}\beta V_{opt}^2 R_{opt}$, of difficult interpretation within the standard theory of galaxy formation. Crucial insight has come from disk–halo density decompo-

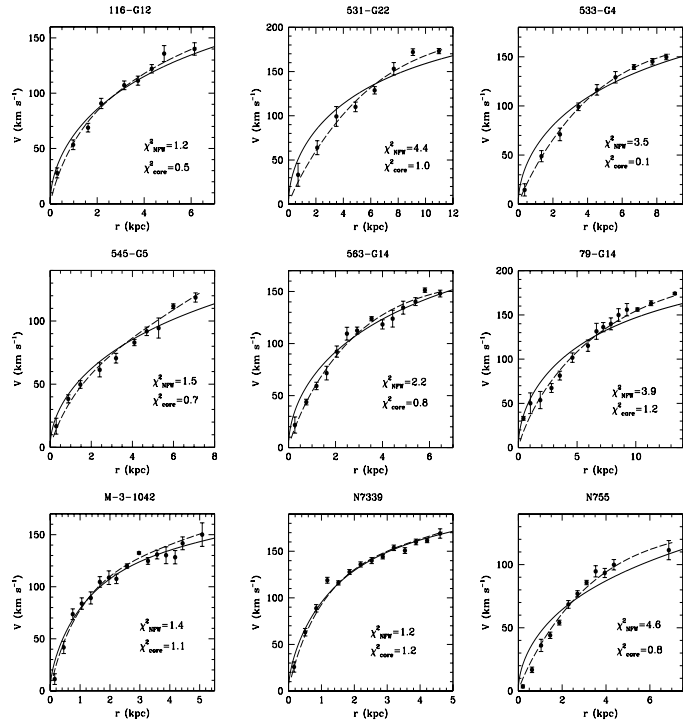


Fig. 8. NFW best-fits solid lines of the rotation curves (filled circles) compared with the CDR fits (dashed lines). The χ^2 values are also indicated

sitions of a number of disk galaxies. These galaxies have a relevant amount of dark matter: the contribution of the luminous matter to the dynamics is small and it can be easily taken into account. Moreover, the high spatial resolution of the available rotation curves allows us to derive the separate dark and luminous density profiles. We find that dark matter halos have a constant central density region whose size exceeds the stellar disk length-scale R_d . As result, the

halo profiles disagree with the cuspy density distributions typical of CDM halos which, therefore, fail to account for the actual DM velocity data.

Pointing out that a review on the various efforts aimed to cope with the core radii evidence will be published elsewhere, we conclude by stressing that, for *any* theory of galaxy formation, time is come to seriously consider that stellar disks (and perhaps also stellar spheroids) lay down in dark halos of constant density.

References

1. A. Borriello, P. Salucci: MNRAS *in press* astro-ph/ (2000)
2. J.S. Bullock, T.S. Kolatt, Y. Sigad, R.S. Somerville, A.V. Kravtsov, A.A. Klypin, J.R. Primack, A. Dekel: MNRAS *in press* astro-ph/9908159 (2000)
3. A. Burkert: ApJ, **447**, L25 (1995)
4. A. Burkert, J. Silk: ApJ, **488**, L55 (1997)
5. S. Burles, D. Tytler: Space Sci. Rev., **84**, 65 (1998)
6. S. Cole, C. Lacey: MNRAS, **281**, 716 (1997)
7. E. Corbelli, P. Salucci: MNRAS, **311**, 411C (2000)
8. R. Flores, J.R. Primack: ApJ, **427**, L1 (1994)
9. K.C. Freeman: ApJ, **160**, 811F (1970)
10. T. Fukushige, J. Makino: ApJ, **477**, L9 (1997)
11. A.V. Kravtsov, A.A. Klypin, J.S. Bullock, J.R. Primack: ApJ, **502**, 48 (1998)
12. S.S. McGaugh, W.J.G. de Block: ApJ, **499**, 41 (1998)
13. B. Moore: Nature, **370**, 629 (1994)
14. B. Moore, F. Governato, T. Quinn, J. Stadel, G. Lake: ApJ, **499**, L5 (1998)
15. J.F. Navarro, C.S. Frenk, S.D.M. White: MNRAS, **275**, 56 (1995)
16. J.F. Navarro, C.S. Frenk, S.D.M. White: ApJ, **462**, 563 (1996)
17. J.F. Navarro, C.S. Frenk, S.D.M. White: ApJ, **490**, 493 (1997)
18. M. Persic, P. Salucci: MNRAS, **245**, 577 (1990b)
19. M. Persic, P. Salucci: ApJS, **99**, 501.. (1995)
20. M. Persic, P. Salucci, F. Stel: MNRAS, **281**, 27P (1996)
21. M.-H. Rhee: PhD thesis, Groningen University (1996)
22. D. F. Roscoe: A&A , **343**, 788 ((1999))
23. P. Salucci: MNRAS *in press* astro-ph/0007389 (2000)
24. P. Salucci, C. Ratnam, P. Monaco, L. Danese: MNRAS, **317**, 488S (2000)
25. P. Salucci, A. Burkert: ApJ, **537L**, 9S (2000)
26. P. Salucci, M. Persic: MNRAS, **309**, 923 (1999)
27. J. Stil: Ph.D. Thesis, Leiden University (1999)
28. T.S. van Albada, J.S. Bahcall, K. Begeman, R. Sancisi: ApJ, **295**, 305 (1985)
29. F.C. van den Bosch, B.E. Robertson, J. Dalcanton, W.J.G. de Blok: AJ , **119**, 1579V (2000)